Inorganic Chemistry
Article

Inorg. Chem. **2010**, *49*, 6077–6084 **6077**
DOI: 10.1021/ic100633w

Efficient Dipyrrin-Centered Phosphorescence at Room Temperature from Bis-Cyclometalated Iridium(III) Dipyrrinato Complexes

Kenneth Hanson, Arnold Tamayo, Vyacheslav V. Diev, Matthew T. Whited, Peter I. Djurovich, and Mark E. Thompson*

Department of Chemistry, University of Southern California, Los Angeles, California 90089

Received April 2, 2010

A series of seven dipyrrin-based bis-cyclometalated Ir(III) complexes have been synthesized and characterized. All complexes display a single, irreversible oxidation wave and at least one reversible reduction wave. The electrochemical properties were found to be dominated by dipyrrin centered processes. The complexes were found to display room temperature luminescence with emission maxima ranging from 658 to 685 nm. Through systematic variation of the cyclometalating ligand and the meso substituent of the dipyrrin moiety, it was found that the observed room temperature emission was due to phosphorescence from a dipyrrin-centered triplet state with quantum efficiencies up to 11.5%. Bis-cyclometalated Ir(III) dipyrrin based organic light emitting diodes (OLEDs) display emission at 682 nm with maximum external quantum efficiencies up to 1.0%.

Introduction

Since their initial synthesis by Hans Fischer in 1934,[1] complexes with dipyrrinato (dipy) ligands have been widely studied because of their synthetic utility as porphyrin precursors and their rich photophysical properties.[2] Interest in the photophysics of these complexes continues to grow predominantly thanks to the discovery of the highly absorptive, strongly emissive boron difluoride dipyrrinato complex (BODIPY)[3] and its more recent applications as a biological label, tunable laser dye, and dopant in electroluminescent devices.[4] In addition to BODIPY, the monoanionic dipyrrinato ligand has been used as a bidentate chelate for numerous metal cations including Cr(III), Mn(II + III), Fe(II + III), Pd(II), Rh(II),[2] and more recently Ru(II),[5,6] Rh(III),[7] and Ir(III).[8]

While a vast number of emissive BODIPY dyes have been prepared, there are very few reports of luminescent dipyrrinato compounds where the ligand is coordinated to a metal cation. Prior examples include complexes with Zn(II),[9,10] Rh(III)[7] and group 13 ions (Al(III),[11] Ga(III), or In(III)[12]). The majority of the metal dipyrrinato complexes are nonemissive, and little is known about the triplet excited state of these species. In fact, one of the attractive features noted for efficient fluorescence from BODIPY dyes is the negligible intersystem crossing into the triplet state.[4] Phosphorescence from the dipyrrinato dyes has been observed at 77 K through formation of the triplet excited state either by charge separation and then recombination,[13] triplet energy transfer,[14] or sensitization by a heavy atom solvent.[15] To facilitate the investigation of the triplet properties of the dipyrrinato ligand it is important to efficiently produce a triplet excited state so that room temperature phosphorescence can be observed.

Recently, room temperature phosphorescence from dipy (Φ = 0.013) has been observed by coordinating the ligand directly to a platinum(II) cyclometalate (C^N) complex.[16] Much like platinum(II) cyclometalates, tris- and bis-cyclometalated iridium(III) complexes are known to have

*To whom correspondence should be addressed. E-mail: met@usc.edu.

(1) Fischer, H.; Orth, H. *Die Chemie des Pyrrols*; Akademische Verlagsgesellschaft: Leipzig, Germany, 1937; Vol. *2*.
(2) Wood, T. E.; Thompson, A. *Chem. Rev.* **2007**, *107*, 1831–1861.
(3) Treibs, A.; Kreuzer, F.-H. *Liebigs Ann. Chem.* **1968**, *718*, 208–223.
(4) Ulrich, G.; Ziessel, R.; Harriman, A. *Angew. Chem., Int. Ed.* **2008**, *47*, 1184–1201.
(5) Smalley, S. J.; Waterland, M. R.; Telfer, S. G. *Inorg. Chem.* **2009**, *48*, 13–15.
(6) Yadav, M.; Singh, A. K.; Maiti, B.; Pandey, D. S. *Inorg. Chem.* **2009**, *48*, 7593–7603.
(7) Hall, J. D.; McLean, T. M.; Smalley, S. J.; Waterland, M. R.; Telfer, S. G. *Dalton Trans.* **2010**, *39*, 437–445.
(8) Yadav, M.; Singh, A. K.; Pandey, D. S. *Organometallics* **2009**, *28*, 4713−4723.
(9) Sutton, J. M.; Rogerson, E.; Wilson, C. J.; Sparke, A. E.; Archibald, S. J.; Boyle, R. W. *Chem. Commun.* **2004**, 1328–1329.
(10) Sazanovich, I. V.; Kirmaier, C.; Hindin, E.; Yu, L.; Bocian, D. F.; Lindsey, J. S.; Holten, D. *J. Am. Chem. Soc.* **2004**, *126*, 2664–2665.
(11) Ikeda, C.; Ueda, S.; Nabeshima, T. *Chem. Commun.* **2009**, 2544–2546.
(12) Thoi, V. S.; Stork, J. R.; Magde, D.; Cohen, S. M. *Inorg. Chem.* **2006**, *45*, 10688–10697.
(13) Galletta, M.; Campagna, S.; Quesada, M.; Ulrich, G.; Ziessel, R. *Chem. Commun.* **2005**, 4222–4224.
(14) Nastasi, F.; Puntoriero, F.; Campagna, S.; Diring, S.; Ziessel, R. *Phys. Chem. Chem. Phys.* **2008**, *10*, 3982–3986.
(15) Harriman, A.; Rostron, J. P.; Cesario, M.; Ulrich, G.; Ziessel, R. *J. Phys. Chem. A* **2006**, *110*, 7994–8002.
(16) Bronner, C.; Baudron, S. A.; Hosseini, M. W.; Strassert, C. A.; Guenet, A.; De Cola, L. *Dalton Trans.* **2010**, *39*, 180−184.

Published on Web 06/08/2010

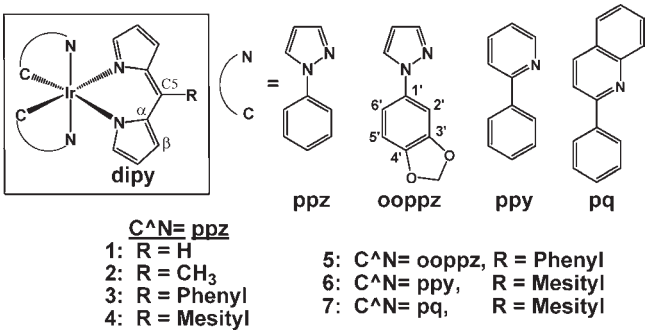

Figure 1. Structure of $(C^N)_2Ir(5\text{-R-dipy})$ complexes **1**−**7**. See Scheme 1 for the isomers of **5**.

long-lived excited states and highly efficient phosphorescent emission. The high efficiency emission is attributed to intersystem crossing from the singlet to the triplet excited state facilitated by strong spin−orbit coupling of the iridium heavy atom.[17] Although a series of $(\eta^5\text{-}C_5Me_5)IrL(5\text{-}(4\text{-R-Ph})dipy)$ (L = Cl, phosphino, 2,2′-bipyridyl; R = CN, NO_2) complexes have been recently prepared,[8] these derivatives were reported to be non-emissive. In this report we describe the synthesis and characterization of a series of bis-cyclometalated Ir(III) compounds containing dipyrrinato ligands (Figure 1) that exhibit phosphorescence at room temperature. Through systematic variation of the cyclometalating ligand and the meso substituent of the dipyrrin moiety, it was found that the photochemical and electrochemical properties were dictated by the dipyrrinato ligand.

Experimental Section

Synthesis. Mesitylaldehyde, benzaldehyde, acetaldehyde, pyrrole, pyrazole, trifluoroacetic acid, indium(III) chloride, 1-phenylpyrazole, 2-phenylpyridine, 2-phenylquinoline, (Aldrich), paraformaldehyde (Fisher), 5-iodo-1,3-benzodioxole (Matrix Scientific), and $IrCl_3 \cdot nH_2O$ (Next Chimica) were purchased from the corresponding supplier (in parentheses) and used without further purification. NMR spectra were recorded on a Bruker AM 360 MHz or Varian 400 MHz NMR instrument as indicated, and chemical shifts were referenced to residual protonated solvent. Elemental analyses (CHN) were performed at the Microanalysis Laboratory at the University of Illinois, Urbana−Champaign. High-performance liquid chromatography (HPLC) analysis was performed on a Shimadzu Prominance-LCMS 2020 equipped with a column oven (T = 40 °C), a PDA photodetector, and a MS spectrometer (LCMS 2020; m/z range: 0−2000; ionization modes: ESI/APCI). HPLC was performed using an Inertsil ODS-3 C18 3 μ 3 × 150 mm column eluting with a 75:25 mixture of acetonitrile and water.

Dipyrromethane,[18] 5-methyl-dipyrromethane,[18] 5-phenyl-dipyrromethane,[19] and 5-mesityl-dipyrromethane[19] were prepared following procedures developed by Lindsey et al. 1-(4,5-Methylenedioxopheny)pyrazole was prepared by Ullmann-type coupling of 5-Iodo-1,3-benzodioxole with pyrazole.[20] Cyclometalated Ir(III) dichloro-bridged dimers of general formula $[(C^N)_2Ir(\mu\text{-Cl})]_2$ were synthesized by heating $IrCl_3 \cdot H_2O$ to 110 °C with 2−2.5 equiv of cyclometalating ligand in a 3:1 mixture of 2-ethoxyethanol and deionized water as previously reported by Nonoyama.[21]

Synthesis of $(C^N)_2Ir$(dipyrrinato) Complexes. To a solution of dipyrromethane (0.5 mmol) in 20 mL of dry tetrahydrofuran (THF) was added (0.5 mmol) 2,3-dicloro-5,6-dicyano-1,4-benzoquinone (DDQ) and allowed to stir at room temperature for 1 h. A large excess of potassium carbonate (1 g) was then added, and the mixture was stirred for 15 min followed by the addition of $[(C^N)_2Ir(\mu\text{-Cl})]_2$ (0.25 mmol). The solution was then refluxed under N_2 overnight. After cooling to room temperature, solids were removed by vacuum filtration and washed with dichloromethane (3 × 50 mL). The collected filtrate was then evaporated to dryness under reduced pressure. The crude product was then passed through a silica gel column using dichloromethane/hexane (9:1) as eluent. Solvent from the first orange fraction was then evaporated to dryness under reduced pressure. The pure product was precipitated with methanol (CH_3OH), collected by filtration, washed with CH_3OH, and air-dried.

Iridium(III) Bis(1′-phenylpyrazolato-N,C$^{2'}$)(dipyrrinato) (1). Yield: 7% ^{1}H NMR (400 MHz, $CDCl_3$), δ 6.29 (dd, J = 4.0, 1.0 Hz, 2H), 6.39−6.41 (m, 4H), 6.78 (td, J = 7.5, 1.0 Hz, 2H), 6.86 (d, J = 1.0 Hz, 2H), 6.91 (dd, J = 7.5, 1.0 Hz, 2H), 6.94 (d, J = 2.0 Hz, 2H), 6.97 (dd, J = 4.0 Hz, 2H), 7.17 (d, J = 8.0 Hz, 2H), 7.31 (s, 1H), 7.96 (d, J = 2.0 Hz, 2H). ^{13}C NMR (100 MHz, $CDCl_3$) δ 106.9, 110.4, 116.8, 121.4, 125.1, 125.7, 130.5, 133.8, 134.2, 134.4, 137.7, 144.0, 151.8. Elemental analysis for $C_{27}H_{21}N_6Ir$: calcd: C 52.16, H 3.40, N 13.52; found: C 51.47, H 3.40, N 12.72.

Iridium(III) Bis(1′-phenylpyrazolato-N,C$^{2'}$)(5-methyldipyrrinato) (2). Yield: 13% ^{1}H NMR (400 MHz, $CDCl_3$), δ 2.76 (s, 3H), 6.30 (dd, J = 4.0, 1.0 Hz, 2H), 6.36 (dd, J = 7.5, 1.0 Hz, 2H), 6.39 (t, J = 3.0 Hz, 2H), 6.77 (td, J = 7.5, 1.0 Hz, 2H), 6.89−6.93 (m, 6H), 7.18 (d, J = 8.0 Hz, 2H), 7.29 (dd, J = 4.0, 1.0 Hz, 2H), 7.94 (d, J = 3.0 Hz, 2H). ^{13}C NMR (100 MHz, $CDCl_3$) δ 19.4, 106.8, 110.4, 116.2, 121.2, 125.0, 125.7, 126.7, 134.1, 135.1, 137.6, 138.3, 143.8, 145.0, 151.1. Elemental analysis for $C_{28}H_{23}N_6Ir$: calcd: C 52.90, H 3.65, N 13.22; found: C 52.75, H 3.54, N 12.93.

Iridium(III) Bis(1′-phenylpyrazolato-N,C$^{2'}$)(5-phenyldipyrrinato) (3). Yield: 70% ^{1}H NMR (400 MHz, $CDCl_3$), δ 6.23 (dd, J = 2.5, 1.5 Hz, 2H), 6.39 (dd, J = 7.5, 1.0 Hz, 2H), 6.46 (t, J = 2.5 Hz, 2H), 6.49 (dd, J = 4.5, 1.5 Hz, 2H), 6.78 (td, J = 7.5, 1.0 Hz, 2H), 6.93 (td, J = 7.5, 1.5 Hz, 2H), 6.99 (t, J = 1.5 Hz, 2H), 7.00 (d, J = 1.5 Hz, 2H), 7.19 (dd, J = 8.0, 1.0 Hz, 2H), 7.37−7.47 (m, 5H), 7.99 (dd, J = 3.0, 1.0 Hz, 2H). ^{13}C NMR (100 MHz, $CDCl_3$) δ 106.9, 110.5, 116.5, 121.3, 125.1, 125.8, 126.9, 127.9, 130.5, 130.9, 134.2, 135.1, 137.6, 137.9, 139.7, 143.9, 148.3, 152.1. Elemental analysis for $C_{33}H_{25}N_6Ir$: calcd: C 56.80, H 3.61, N 12.04; found: C 56.69, H 3.22, N 11.93.

Iridium(III) Bis(1′-phenylpyrazolato-N,C$^{2'}$)(5-mesityldipyrrinato) (4). Yield: 73% ^{1}H NMR (400 MHz, $CDCl_3$), δ 2.06 (s, 6H), 2.36 (s, 3H), 6.16 (dd, J = 4.0, 1.5 Hz, 2H), 6.38 (dd, J = 4.0, 1.5 Hz, 2H), 6.42−6.45 (m, 4H), 6.79 (td, J = 7.5, 1.0 Hz, 2H), 6.90−6.95 (m, 6H), 7.01 (d, J = 2.0 Hz, 2H), 7.19 (dd, J = 8.0, 1.0 Hz, 2H), 7.99 (d, J = 2.0 Hz, 2H). ^{13}C NMR (100 MHz, $CDCl_3$) δ 19.8, 21.1, 106.9, 110.5, 116.5, 121.3, 125.1, 125.8, 127.4, 129.3, 134.26, 134,28, 136.1, 136.3, 136.7, 137.5, 138.1, 144.0, 147.2, 151.6. Elemental analysis for $C_{36}H_{31}N_6Ir$: calcd: C 58.44, H 4.22, N 11.36; found: C 58.26, H 3.74, N 11.02.

Iridium(III) Bis[1′-(4,5-methylenedioxophenyl)pyrazolato-N,C$^{2'}$](5-phenyldipyrrinato), Iridium(III) [1′-(4,5-methylenedioxophenyl)pyrazolato-N,C$^{2'}$][1′-(4,5-methylenedioxophenyl)pyrazolato-N,C$^{6'}$](5-phenyldipyrrinato), Iridium(III) Bis[1′-(4,5-methylenedioxophenyl)pyrazolato-N,C$^{6'}$](5-phenyldipyrrinato) (5(2′,2′), 5-(2′,6′), and 5(6′,6′), Respectively). Yield: 58% Product was further purified by sublimation under reduced pressure. All characterization reported herein were performed on a sublimed sample. ^{1}H NMR (400 MHz, $CDCl_3$), δ 7.90 (dd, J = 2.8, 0.8 Hz, 2H), δ 7.84

(17) Yersin, H. *Highly efficient OLEDs with phosphorescent materials*; Wiley-VCH: Berlin, 2007.
(18) Laha, J. K.; Dhanalekshmi, S.; Taniguchi, M.; Ambroise, A.; Lindsey, J. S. *Org. Process Res. Dev.* **2003**, *7*, 779–812.
(19) Littler, B. J.; Miller, M. A.; Hung, C.-H.; Wagner, R. W.; O'Shea, D. F.; Boyle, P. D.; Lindsey, J. S. *J. Org. Chem.* **1999**, *64*, 1391–1396.
(20) Klapars, A.; Antilla, J. C.; Huang, X.; Buchwald, S. L. *J. Am. Chem. Soc.* **2001**, *123*, 7727–7729.
(21) Nonoyama, M. *Bull. Chem. Soc. Jpn.* **1974**, *47*, 767–768.

(dd, J = 2.8, 0.8 Hz, 2H), δ 7.83 (dd, J = 2.8, 0.8 Hz, 2H), δ 7.76 (dd, J = 2.8, 0.8 Hz, 2H), 7.50−7.35 (m, 20H), 7.14 (t, J = 1.2 Hz, 2H), 7.12 (t, J = 1.2 Hz, 2H), 7.05 (t, J = 1.2 Hz, 2H), 7.03 (t, J = 1.2 Hz, 2H), 6.93 (dd, J = 2.8, 0.8 Hz, 2H), 6.91 (dd, J = 2.8, 0.8 Hz, 2H), 6.87 (dd, J = 2.8, 0.8 Hz, 2H), 6.85 (dd, J = 2.8, 0.8 Hz, 2H), 6.84 (s, 2H), 6.83 (s, 2H), 6.80 (d, J = 8 Hz, 2H), 6.78 (d, J = 8 Hz, 2H), 6.52−6.48 (m, 8H), 6.46 (d, J = 8 Hz, 2H), 6.45 (d, J = 8 Hz, 2H), 6.41−6.38 (m, 4H), 6.31−6.28 (m, 4H), 6.28−6.23 (m, 8H), 5.88 (d, J = 1.6 Hz, 2H), 5.87 (d, J = 1.6 Hz, 2H), 5.81 (d, J = 1.6 Hz, 2H), 5.80 (d, J = 1.6 Hz, 2H), 5.79 (s, 2H), 5.76 (s, 2H), 5.60 (d, J = 1.6 Hz, 2H), 5.58 (d, J = 1.6 Hz, 2H), 5.43 (d, J = 1.6 Hz, 2H), 5.40 (d, J = 1.6 Hz, 2H). ^{13}C NMR (100 MHz, $CDCl_3$) δ 153.3, 152.6, 152.2, 152.1, 151.7, 148.3, 145.27, 145.0, 143.5, 143.3, 142.9, 142.8, 141.0, 140.4, 139.6, 139.5, 139.4, 138.3, 138.1, 137.2, 137.0, 136.4, 135.0, 134.9, 134.5, 134.4, 130.9, 130.8, 130.5, 130.4, 130.0, 128.6, 128.0, 127.9, 127.8, 126.9, 124.9, 124.6, 124.0, 123.7, 116.8, 116.7, 116.4, 116.3, 116.1, 114.7, 113.3, 113.1, 106.9, 106.7, 106.0, 105.8, 104.2, 103.9, 101.5, 101.4, 100.4, 100.3, 99.6, 99.5, 93.9, 93.7. Elemental analysis for $C_{35}H_{25}N_6O_4Ir$: calcd: C 53.49, H 3.21, N 10.69; found: C 53.16, H 2.84, N 10.42.

Iridium(III) Bis(2-phenylpyridinato-N,C$^{2'}$)(5-mesityldipyrrinato) (6). Yield: 66% ^{1}H NMR (360 MHz, $CDCl_3$), δ 7.89 (ddd, J = 5.9, 1.5, 0.7 Hz, 2H), 7.80 (dd, J = 8.05, 5.9 Hz, 2H), 7.61−7.54 (m, 4H), 6.90 (ddd, J = 7.8, 7.3, 1.5 Hz, 2H), 6.88 (s, 2H), 6.85 (ddd, J = 7.6, 5.8, 1.5 Hz, 2H), 6.81 (ddd, J = 7.8, 7.3, 1.5 Hz, 2H), 6.71 (dd, J = 1.7, 1.2 Hz, 2H), 6.41 (dd, J = 7.6, 1.2 Hz, 2H), 6.37 (dd, J = 4.2, 1.5 Hz, 2H), 6.14 (dd, J = 4.4, 1.2 Hz, 2H), 2.34 (s, 3H), 2.02 (s, 6H); ^{13}C NMR (90 MHz, $CDCl_3$) δ 168.8, 156.8, 151.8, 149.6 (2C), 147.3, 144.5, 136.7, 136.2, 135.9, 133.6, 132.3, 129.5 (2C), 127.4, 123.8, 121.6, 120.7, 118.6, 116.9. Elemental analysis for $C_{40}H_{33}N_4Ir$: calcd: C 63.05, H 4.37, N 7.35; found: C 62.90, H 4.11, N 7.37.

Iridium(III) Bis(2-phenylquinalato-N,C$^{2'}$)(5-mesityldipyrrinato) (7). Yield: 71.5% ^{1}H NMR (360 MHz, $CDCl_3$), δ 8.06 (dd, J = 10.3, 8.8 Hz, 2H), 8.03 (dd, J = 10.3, 8.8 Hz, 2H), 7.81 (d, J = 3.4 Hz, 2H), 7.79 (d, J = 4.6 Hz, 2H), 7.66 (dd, J = 8.1, 1.5 Hz, 2H), 7.31 (dd, J = 8.1, 7.3 Hz, 2H), 7.06 (ddd, J = 9.3, 7.8, 1.5 Hz, 2H), 6.96 (dd, J = 8.3, 7.3 Hz, 2H), 6.72 (s, 2H), 6.70 (dd, J = 8.3, 7.3 Hz, 2H), 6.61 (d, J = 1.9 Hz, 2H), 6.47 (d, J = 7.6 Hz, 2H), 6.24 (dd, J = 4.4, 1.0 Hz, 2H), 6.11 (dd, J = 4.2, 1.0 Hz, 2H), 2.26 (s, 3H), 1.45 (s, 6H); ^{13}C NMR (90 MHz, $CDCl_3$), δ 171.21, 164.84, 157.93, 150.06, 149.18, 147.30, 146.930, 138.22, 136.50, 136.44, 136.09, 134.49, 133.94, 130.26, 129.80, 129.65, 127.94, 127.70, 127.47, 127.14, 125.86, 125.71, 120.86, 117.06, 21.02, 19.23. Elemental analysis for $C_{48}H_{37}N_4Ir\cdot CH_2Cl_2$: calcd: C 62.15, H 4.15, N 5.92; found: C 62.57, H 4.05, N 6.08.

X-ray Crystallography. Diffraction data for compounds **3**, **4**, and **5**(6′,6′) were collected on a Bruker SMART APEX CCD diffractometer with graphite monochromated Mo Kα radiation (λ = 0.71073 Å). The cell parameters for the complexes were obtained from a least-squares refinement of the spots (from 60 collected frames) using the SMART program. One hemisphere of crystal data for each compound was collected up to a resolution of 0.80 Å, and the intensity data were processed using the Saint Plus program. All of the calculations for the structure determination were carried out using the SHELXTL package (Version 5.1).[22] Absorption corrections were applied by using SADABS.[23] In most cases, hydrogen positions were input and refined in a riding manner along with the attached carbons. A summary of the refinement details and the resulting factors are given in Supporting Information, Table 1.

Electrochemical and Photophysical Characterization. Cyclic voltammetry (CV) and differential pulse voltammetry (DPV) were performed using an EG&G Potentiostat/Galvanostat model 283. *N*,*N*-dimethylformamide (DMF, purchased from VWR) was used as the solvent under inert atmosphere with 0.1 M tetra(*n*-butyl)ammonium hexafluorophosphate (Aldrich) as the supporting electrolyte or a solution of anhydrous 0.1 M NBu_4ClO_4 in CH_2Cl_2 (VWR) as indicated. A glassy carbon rod, a platinum wire, and a silver wire were used as the working electrode, the counter electrode, and the pseudo reference electrode, respectively. Electrochemical reversibility was established using CV, while all redox potentials were determined using DPV and reported relative to a ferrocenium/ferrocene (Fc^+/Fc) redox couple used as an internal standard.[24]

The UV−visible spectra were recorded on a Hewlett-Packard 4853 diode array spectrophotometer. Steady state emission experiments at room temperature and 77 K were performed using a Photon Technology International QuantaMaster Model C-60SE spectrofluorimeter. Phosphorescence lifetime measurements were performed by a time-correlated single-photon counting method using an IBH Fluorocube lifetime instrument by equipped with a 405 nm LED excitation source. Quantum efficiency measurements were carried out using a Hamamatsu C9920 system equipped with a xenon lamp, calibrated integrating sphere and model C10027 photonic multichannel analyzer.

Computational Methods. All calculations were performed using the Titan software package (Wavefunction, Inc.). The gas phase geometry optimizations were calculated using B3LYP functional with the LACVP** basis set as implemented in Titan. The energy levels and orbital diagrams of the highest occupied molecular orbital (HOMO) and lowest unoccupied molecular orbital (LUMO) were obtained from the optimized geometry of the singlet state. The spin-density of the triplet state was calculated from the energy minimized triplet geometries.

Device Fabrication. Prior to device fabrication, indium/tin oxide (ITO) on glass was patterned as 2-mm-wide stripes with a resistivity of 20 $\Omega\,\square^{-1}$. The substrates were cleaned by sonication in a soap solution, rinsed with deionized water, boiled in trichloroethylene, acetone, and ethanol for 5−6 min in each solvent, and dried with nitrogen. Finally, the substrates were treated with UV ozone for 10 min. Layers of NPD (400 Å), 10% **3** or **5** doped into Alq_3 (250 Å) and BCP (400 Å) were vapor-deposited onto the substrates in a high-vacuum chamber. Lithium fluoride (10 Å) and aluminum (1200 Å) were then vapor-deposited onto the substrates through a shadow mask, that defined four devices per substrate with a 2-mm^2 active area each, in the same high-vacuum chamber. The devices were tested within 3 h of fabrication. The electrical and optical intensity characteristics of the devices were measured with a Keithly 2400 source/meter/2000 multimeter coupled to a Newport 1835-C optical meter, equipped with a UV-818 Si photodetector. Only light emitting from the front face of the device was collected and used in subsequent efficiency calculations. The electroluminescent (EL) spectra were measured on a PTI QuantaMaster model C-60SE spectrofluorimeter, equipped with a 928 PMT detector and corrected for detector response.[25] The EL intensity was found to be uniform throughout the area of each device.

Results and Discussion

Synthesis and Structure. The bis-cyclometalated Ir(III) dipyrrinato complexes (Figure 1) were prepared by a modified "one-pot" procedure introduced by Lindsey for bis(dipyrrinato)metal complexes.[26] In a stepwise manner, dipyrromethane was first oxidized using DDQ followed by sequential addition of K_2CO_3 and cyclometalated Ir(III)

(22) Sheldrick, G. M. *SHELXTL*, Version 5.1; Bruker Analytical X-ray System, Inc: Madison, WI, 1997.

(23) Blessing, R. H. *Acta Crystallogr., Sect. A* **1995**, *51*, 33–38.

(24) Gagne, R. R.; Koval, C. A.; Lisensky, G. C. *Inorg. Chem.* **1980**, *19*, 2854–2855.

(25) Forrest, S. R.; Bradley, D. D. C.; Thompson, M. E. *Adv. Mater.* **2003**, *15*, 1043–1048.

(26) Yu, L.; Muthukumaran, K.; Sazanovich, I. V.; Kirmaier, C.; Hindin, E.; Diers, J. R.; Boyle, P. D.; Bocian, D. F.; Holten, D.; Lindsey, J. S. *Inorg. Chem.* **2003**, *42*, 6629–6647.

Scheme 1

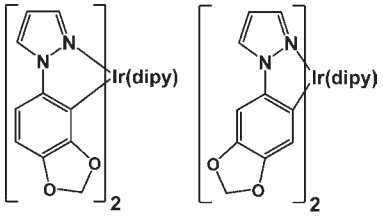

5(2',2') 5(6',6')

dichloro-bridged dimers to give complexes **3**−**7** in 50−75% yield. Using the same synthetic method, complexes **1** and **2** were obtained in 5−15% yield. The lower yields for complexes **1** and **2** (comparable to those found for the boron difluoride analogues[27,28]) are likely due to thermal instability[29] of the dipyrrin intermediate under the given reaction conditions (refluxing THF).

All of the complexes were fully characterized by ^{1}H and ^{13}C NMR spectroscopy and elemental analysis. The relatively simple NMR spectra of complexes **1**−**4**, **6**, and **7** are indicative of a C_2-symmetric species having the same trans-N disposition for the C^N chelate as the dimeric Ir starting material. However, the NMR spectra of (ooppz)$_2$-Ir(5-Ph-dipy) (**5**) was more complex. Analysis by HPLC-MS indicated the presence of three species, in an approximate 1:2:1 ratio, which had identical mass and similar absorption spectra (Supporting Information, Figure S16). Using a combination of ^{1}H−^{1}H COSY (Supporting Information, Figure S10) and ^{1}H−^{1}H decoupled NMR (Supporting Information, Figure S11), along with comparison to ^{1}H NMR spectra of complexes **1**−**4**, three regioisomeric forms of **5** were established: bis(2′-ooppz)Ir(5-Ph-dipy) **5**(2′,2′), (2′-ooppz)(6′-ooppz)Ir(5-Ph-dipy) **5**(2′,6′), and bis(6′-ooppz)Ir-(5-Ph-dipy) **5**(6′,6′) (Scheme 1). The statistical ratio of the regioisomers indicates that there is no preference for either the 2′ or 6′ positions during cyclometalation of the ooppz ligand.

Crystals of complexes **3**, **4**, and **5**(6′,6′) suitable for X-ray diffraction analysis were obtained by zone sublimation. The structures show ligands arranged in a pseudo-octahedral geometry around the metal center with the expected *trans*-configuration of pyrazolyl groups (Figure 2). Bond lengths and angles for the C^N ligands are comparable to those found in literature for similar heteroleptic complexes (Supporting Information, Table S2).[30] Likewise, the bond lengths and angles of the dipyrrinato moiety are similar to those of other metal dipyrrinato-based complexes. The iridium-pyrrolic nitrogen (M−N$_{pyr}$) bond lengths (Ir−N$_{pyr}$ ≈ 2.11 Å) are comparable to those found in the (η^5-C$_5$Me$_5$)Ir-(Ph$_3$P)(5-(4-NO$_2$Ph)dipy) complex (Ir−N = 2.074(5) and 2.090(5)). Similar distances have also been observed in (ppy)Pt(5-mesityldipy) complex where the Pt−N$_{pyr}$ bond lengths are 2.091(6) Å and 2.027(6) Å.

The two pyrrole rings in complexes **3**, **4**, and **5**(6′,6′) are not coplanar, unlike what is observed for dipyrrinato ligands in boron,[31] zinc,[26] and iron[32] complexes. Instead, the dipyrrinato ligand is bent in a manner similar that seen in Co(III)[33] and Pd(II)[7,34] complexes. This distortion of the pyrrole rings is defined here using a fold-angle between the planes formed by the nitrogen, α and β carbon atoms adjacent to the C5 carbon (Figure 1 and Supporting Information, Figure S17). Fold-angles of 17.9(2)° and 17.7(5)° are found in complexes **3** and **5**(6′,6′), respectively, while **4** contains two unique molecules in the asymmetric unit cell, one with a bent dipyrrinato ligand (fold-angle = 11.1(9)°), the other near planar (fold-angle = 1.0(8)°). The folding distortion is accompanied by a tilt of the dipyrrinato ligand away from a square plane composed of the two coordinated carbons, iridium center, and two N$_{pyr}$ atoms. This tilt-angle can be quantified using two planes, one defined by the Ir and two N$_{pyr}$ atoms versus the other that includes the two N$_{pyr}$ atoms and the C5 carbon (see Supporting Information, Figure S18). The tilt-angles were found to be 17.3(1)° in **3**, 22.6(2)° in **5**(6′,6′), 14.3(3)° in **4** (bent), and 0.3(3)° in **4** (planar). In addition to the buckling and tilting distortions, a twist of the pendant aryl ring away from an orthogonal conformation was observed. The aryl ring is canted at an angle of 67.5(3)° in **3** and 72.3(5)° in **5**(6′,6′), 74.0(7)° in **4** (bent) and 78.0(7)° in **4** (planar). These out-of-plane distortions in the dipyrrinato ligand appear to require low energy and are likely caused by crystal packing forces since both planar and nonplanar forms of the ligand are present in the structure of **4**.

DFT Calculations. Density functional theory (DFT) calculations of complex **1**−**7** were performed using the B3LYP functional with the LACVP** basis set. Theoretical investigation of cyclometalated iridium complexes using DFT calculations has repeatedly demonstrated good correlation with experimental observations.[35−38] Metrical parameters for the geometry-optimized structures of **3**, **4**, and **5**(6′,6′) are well-correlated with equivalent bond lengths and angles obtained by X-ray crystallography. For example, the calculated bond lengths (Ir−N$_{pyr}$ = 2.18 Å, Ir−N$_{pz}$ = 2.05 Å, and Ir−C$_{Ph}$ = 2.05 Å) and bond angles (N$_{pyr}$−Ir−N$_{pyr}$ = 86.1°, N$_{pz}$−Ir−N$_{pz}$ = 174.4°, and C$_{Ph}$−Ir−N$_{pz}$ = 79.5°) for complex **3** are within 0.06 Å and 1° of the X-ray structure (Supporting Information, Table S2). One notable difference is that the dipyrrinato ligand is planar (fold-angle = 0°) in the calculated geometries, as opposed to bent in the crystal structure.

For complexes **1**−**4**, **6**, and **7**, the calculations show that both valence orbitals are localized on the dipyrrinato

(27) Tram, K.; Yan, H.; Jenkins, H. A.; Vassiliev, S.; Bruce, D. *Dyes Pigm.* **2009**, *82*, 392–395.
(28) Schmitt, A.; Hinkeldey, B.; Wild, M.; Jung, G. *J. Fluoresc.* **2009**, *19*, 755–758.
(29) Van Koeveringe, J. A.; Lugtenburg, J. *Rec. Trav. Chim. Pays-Bas* **1977**, *96*, 55–58.
(30) Tamayo, A. B.; Garon, S.; Sajoto, T.; Djurovich, P. I.; Tsyba, I. M.; Bau, R.; Thompson, M. E. *Inorg. Chem.* **2005**, *44*, 8723–8732.
(31) Li, F.; Yang, S. I.; Ciringh, Y.; Seth, J.; Martin, C. H., III; Singh, D. L.; Kim, D.; Birge, R. R.; Bocian, D. F.; Holten, D.; Lindsey, J. S. *J. Am. Chem. Soc.* **1998**, *120*, 10001–10017.
(32) Cohen, S. M.; Halper, S. R. *Inorg. Chim. Acta* **2002**, *341*, 12–16.
(33) Telfer, S. G.; Wuest, J. D. *Cryst. Growth Des.* **2009**, *9*, 1923–1931.
(34) March, F. C.; Couch, D. A.; Emerson, K.; Fergusso., J. E.; Robinson, W. T. *J. Chem. Soc., A* **1971**, 440–448.
(35) Tamayo, A. B.; Alleyne, B. D.; Djurovich, P. I.; Lamansky, S.; Tsyba, I.; Ho, N. N.; Bau, R.; Thompson, M. E. *J. Am. Chem. Soc.* **2003**, *125*, 7377–7387.
(36) Sajoto, T.; Djurovich, P.; Tamayo, A. B.; Oxgaard, J.; Goddard, W. A., III; Thompson, M. E. *J. Am. Chem. Soc.* **2009**, *131*, 9813–9822.
(37) Nie, D.; Liu, Z.; Bian, Z.; Huang, C. *J. Mol. Struct., THEOCHEM* **2008**, *861*, 97–102.
(38) Lowry, M. S.; Hudson, W. R.; Pascal, R. A., Jr.; Bernhard, S. *J. Am. Chem. Soc.* **2004**, *126*, 14129–14135.

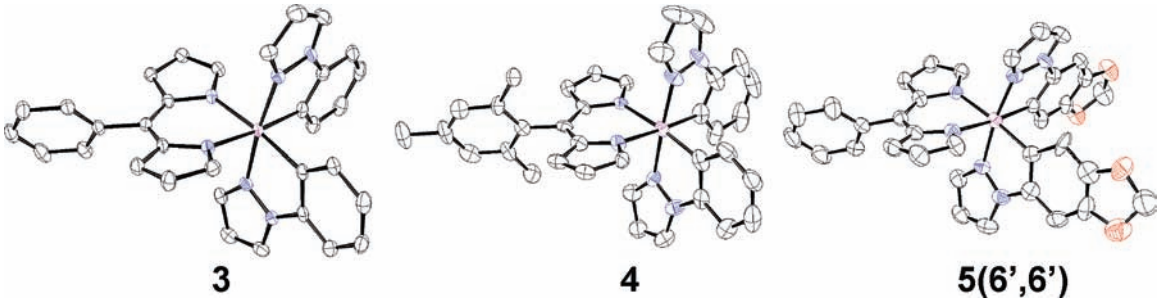

Figure 2. ORTEP drawings of compounds **3**, **4**, and **5**(6′,6′). (carbon (black), nitrogen (blue), oxygen (red), iridium (purple)). A second unique structure for **4** found in the unit cell is not shown.

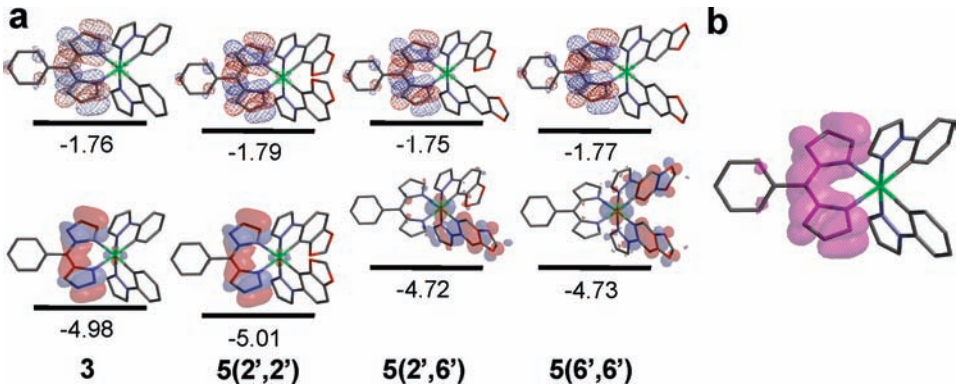

Figure 3. (a) Qualitative orbital energy diagram illustrating the HOMO (transparent) and LUMO (mesh) orbitals of **3** and **5**(2′,2′), **5**(2′,6′), and **5**(6′,6′). All values reported in eV. (b) Triplet spin-density surface of **3**.

ligand. A representative example of the HOMO and LUMO is illustrated for complex **3** in Figure 3a. Roughly similar HOMO (−4.96 to −5.01 eV) and LUMO (−1.71 to −1.79 eV) energies are also calculated for these derivatives (Table 1). Likewise, the LUMOs for the three regioisomers of **5** have similar energy and spatial distribution as the other complexes. However, the HOMOs differ depending on the site of metalation. Cyclometalation at the 2′ position of the ooppz ligand has minimal affect on the location/energy of the HOMO in **5**(2′,2′), whereas cyclometalation at the 6′ position in **5**(6′,6′) and **5**(2′,6′) shifts the HOMO from dipyrrinato to the 6′-ooppz ligand (Figure 3a). The change in location of the HOMO also shifts the orbital energy to more positive values (−4.73 eV). However, these differences in the HOMO character are not reflected in the triplet state. A representative example of the spin density distribution for the HOMO and LUMO is illustrated in Figure 3b for complex **3**. All of the complexes have nearly identical spin density contours that are localized on the dipyrrinato ligand; little-to-no spin density is observed on either the C^N ligand or the iridium atom.

Electrochemistry. The electrochemical properties of the complexes **1**−**7** were investigated using cyclic voltammetry and differential pulsed voltammetry; results of these measurements are listed in Table 1. The complexes all display a reversible reduction wave between −1.89 V and −1.96 V. These potentials are much less cathodic than what is found for related Ir(C^N)$_2$(acetylacetonate) complexes ($E_{1/2}^{red}$ = −3.1 V to −2.45 V)[39] and indicate a reduction process associated with the dipyrrinato ligand. The assignment is consistent with the similarity in the reduction potentials for **1**−**7** (Table 1) and supported by the results from DFT calculations which show closely related LUMO energies for all of the complexes. Two additional reversible reduction peaks were observed with complex **7** at higher potential (−2.46 V and −2.70 V). These processes are assigned to the reduction of the two quinolinyl moieties since they occur at potentials similar to values reported for the (pq)$_2$Ir(acetylacetonate) complex.[40]

Table 1. Calculated HOMO/LUMO Values and Oxidation/Reduction Potentials for Complexes **1**−**7**

	calculation[a]		electrochemistry[b]		
complex	HOMO (eV)	LUMO (eV)	E^{ox} (V)	$E_{1/2}^{red}$ (V)	ΔE (V)
1	−4.99	−1.72	0.52	−1.95	2.47
2	−4.97	−1.71	0.52	−1.98	2.50
3	−4.98	−1.76	0.53	−1.96	2.49
4	−4.98	−1.79	0.55	−1.89	2.44
5(6′,6′)	−4.73	−1.77			
5(2′,6′)	−4.72	−1.75	0.39, 0.56[c]	−1.92 [c]	2.31
5(2′,2′)	−5.01	−1.79			
6	−4.99	−1.80	0.51	−1.91	2.42
7	−4.96	−1.79	0.56	−2.70, −2.46, −1.96	2.52

[a] B3LYP/LACVP**. [b] Redox measurements were performed in an anhydrous 0.1 M NBu_4PF_6 DMF solution and reported relative to internal Fc^+/Fc. [c] Performed on a mixture of regioisomers of **5** in an anhydrous 0.1 M NBu_4ClO_4 CH_2Cl_2 solution.

Complexes **1**−**4**, **6**, and **7** display irreversible oxidation waves from 0.51 to 0.56 V. Irreversible or quasi-reversible

(39) Fei, T.; Gu, X.; Zhang, M.; Wang, C.; Hanif, M.; Zhang, H.; Ma, Y. *Synth. Met.* **2009**, *159*, 113–118.

(40) Wu, F.-I.; Su, H.-J.; Shu, C.-F.; Luo, L.; Diau, W.-G.; Cheng, C.-H.; Duan, J.-P.; Lee, G.-H. *J. Mater. Chem.* **2005**, *15*, 1035–1042.

Table 2. Photophysical Properties of Complexes **1**−**7**

		emission at rt[b]					emission at 77 K[b]	
complex	absorbance λ (nm) (ε, $\times 10^4$ M^{-1} cm^{-1})[a]	λ_{max}(nm)	τ (μs)	Φ_{PL}	k_r(10^4 s^{-1})[c]	k_{nr}(10^5 s^{-1})[d]	λ_{max}(nm)	τ (μs)
1	228 (3.13), 245 (2.94), 311 (0.74), 474 (3.31)	672	12.9	0.075	0.58	0.72	661	23.1
2	229 (3.67), 243 (3.20), 310 (0.82), 480 (3.80)	658	9.9	0.094	0.95	0.92	644	22.3
3	229 (3.67), 244 (3.48), 304 (1.36), 481 (3.52)	683 (675)	5.3 (8.1)	0.060 (0.092)	1.1 (1.1)	1.8 (1.1)	668	16.0
4	228 (4.58), 245 (3.46), 310 (0.76), 483 (3.59)	676 (673)	12.7 (12.6)	0.115 (0.116)	0.91 (0.92)	0.70 (0.70)	664	22.4
5[e]	229 (4.37), 260 (2.88), 300 (2.17), 481 (3.53)	685	4.3	0.060	1.4	2.2	670	16.0
6	246 (3.48), 342 (0.85), 404 (0.94), 483 (3.84)	677	6.3	0.099	1.6	1.4	665	12.9
7	269 (5.03), 342 (1.81), 388 (0.97), 485 (3.60)	675	9.6	0.092	0.96	0.95	659	18.7

[a] In CH_2Cl_2. [b] In 2-MeTHF deaerated with N_2. Data in parentheses recorded in PMMA (2% w/w). [c] $k_r = \Phi/\tau$. [d] $k_{nr} = (1 - \Phi)/\tau$. [e] Mixture of regioisomers.

oxidative processes have also been observed in Fe(5-Ph-dipy)$_3$,[32] Zn(5-Ph-dipy)$_2$,[26] and (η^5-C_5Me_5)IrCl(5-(4-cyanoPh)dipy)[8] at similar potentials. On the other hand, bis- and tris-(C^N) Ir(III) complexes typically undergo a one-electron, reversible oxidation assigned to the metal-aryl ligand portion of the molecules.[35,39,41] The irreversible response for **1**−**4**, **6**, and **7**, and close similarity in potential to other dipyrrinato containing materials, suggests that oxidation is associated with the dipyrrinato ligand. The DFT calculations support this interpretation as they show that the HOMO of **1**−**4**, **6**, and **7** is localized on the dipyrrinato ligand (Figure 3). In contrast, a regioisomeric mixture of **5** displays a reversible oxidation wave at a potential ~130 mV more negative than that of the other complexes (Table 1). Further, a small, irreversible oxidation wave can be resolved at 0.56 V in CH_2Cl_2 (Supporting Information, Figure S19). The data correspond well with the HOMO energies obtained by DFT calculations. Both **5**(6′,6′) and **5**(2′,6′) have HOMOs localized on the C^N, rather than the dipyrrinato ligand (Figure 3) and HOMO energies (−4.73 eV) that are destabilized compared to the other complexes (−4.96 eV to −5.01 eV). For these two isomers, the data indicate that the initial oxidation process is localized on the C^N ligand. The second smaller peak at 0.56 V is tentatively assigned to oxidation of the **5**(2′,2′) regioisomer since the calculations show the HOMO is located at a similar location (dipyrrinato) and energy (−5.01 eV) as complexes **1**−**4**, **6**, and **7**. The lower intensity of this second oxidation wave can be attributed to the lower abundance of the **5**(2′,2′) isomer (~25%) relative to the other two isomers of **5**.

Electronic Spectroscopy. Absorption and emission data for complexes **1**−**7** recorded at room temperature and 77 K are summarized in Table 2. Representative spectra are shown in Figure 4. The absorption spectra of the complexes in dichloromethane show intense bands ($\varepsilon > 10^4$ M^{-1} cm^{-1}) between 200−400 nm that are assigned to both spin-allowed π−π* ligand-centered (LC) and metal-to-ligand charge transfer (MLCT) transitions associated with the C^N ligand (Supporting Information, Figure S20). A distinct feature is a very intense absorption band ($\varepsilon \sim 3.3$−4.0×10^4 M^{-1} cm^{-1}) extending from 400 to 540 nm.

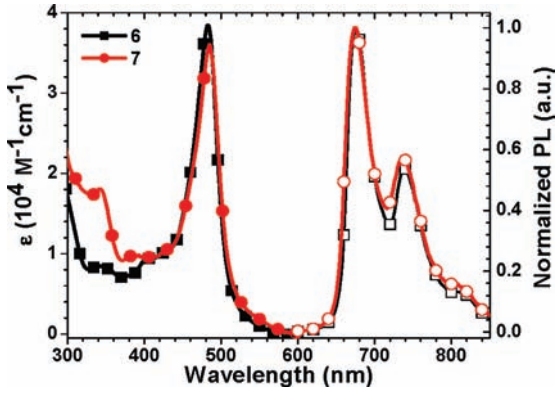

Figure 4. Absorption (in CH_2Cl_2, filled symbol) and emission (in 2-MeTHF, open symbol) spectra of **6** (square) and **7** (circle) at room temperature.

This band has similar absorption intensity and wavelength to boron- and metal-dipyrrinato dyes[5,26,42−44] and is thus assigned to the $^1\pi$−π* ligand-centered transition of the dipyrrinato ligand. The assignment is further supported by comparing derivatives having either different C^N ligands (**4**−**7**) or substituents at the C5 position of the dipyrrinato chromophore (**1**−**4**). Variation in the C^N ligand has minimal affect on the absorption wavelength and intensity of the peak at ~480 nm in complexes **4**−**7** (Figure 4 and Supporting Information, Figure S20b). However, a small red shift (~7 nm) in the peak is observed when the parent dipyrrinato ligand in **1** (λ_{max} = 474 nm) is substituted with either a methyl or aryl group (**2**−**4**). Another feature associated with the dipyrrinato ligand can be observed near 310 nm in complex **3**, where the absorptivity of this peak is nearly double that of **4** (Table 2 and Supporting Information, Figure S20a). A similar enhanced absorbance found in analogous BF_2-dipyrrinato compounds has been attributed to an in-plane rotation of the phenyl group, which increases probability of this transition.[45]

All complexes display vibronically structured luminescence in fluid solution at room temperature and in glassy media at 77 K. The emission peak maxima fall in a narrow range at both room temperature (658−685 nm) and 77 K (644−670 nm), with microsecond lifetimes (room temperature, 5−13 μs; 77 K, 12−23 μs) at 77 K. Lower energy vibrational modes extend out past 800 nm (Figure 4 and Supporting Information, Figure S21). For complexes **1**−**7**, large apparent Stokes shifts (5500−6200 cm^{-1})

(41) Lamansky, S.; Djurovich, P.; Murphy, D.; Abdel-Razzaq, F.; Kwong, R.; Tsyba, I.; Bortz, M.; Mui, B.; Bau, R.; Thompson, M. E. *Inorg. Chem.* **2001**, *40*, 1704–1711.
(42) Loudet, A.; Burgess, K. *Chem. Rev.* **2007**, *107*, 4891–4932.
(43) Wagner, R. W.; Lindsey, J. S. *Pure Appl. Chem.* **1996**, *68*, 1373–1380.
(44) Bruckner, C.; Zhang, Y.; Rettig, S. J.; Dolphin, D. *Inorg. Chim. Acta* **1997**, *263*, 279–286.
(45) Kee, H. L.; Kirmaier, C.; Yu, L.; Thamyongkit, P.; Youngblood, W. J.; Calder, M. E.; Ramos, L.; Noll, B. C.; Bocian, D. F.; Scheidt, W. R.; Birge, R. R.; Lindsey, J. S.; Holten, D. *J. Phys. Chem. B* **2005**, *109*, 20433–20443.

and long excited-state lifetimes are indicative of phosphorescence. In contrast, metal- and boron-containing dipyrrinato complexes typically display fluorescent emission centered around 510 nm with only small Stokes shifts (< 1000 cm^{-1}) from the lowest energy absorption band.[26,42,45]

The Ir complexes all emit at similar wavelength regardless of the cyclometalating ligand. This is best exemplified by comparing the emission spectra of the $(ppy)_2$Ir and $(pq)_2$Ir dipyrrinato complexes (**6** and **7**) to analogous derivatives coordinated with diketonate ligands. Bis-cyclometalated iridium acetylacetonate complexes emit from a triplet state with ^{3}LC/MLCT character at energies that are strongly dependent on the nature of the cyclometalating ligand. As a result, emission maxima of $(ppy)_2$Ir(acac) ($\lambda_{max} = 516$ nm) and $(pq)_2$Ir(acac) ($\lambda_{max} = 597$ nm) differ considerably.[41] In contrast, the emission maxima of **6** and **7** are similar (677 and 675 nm) as can be seen in Figure 4.

Small variations in λ_{max} are found with differing substituents on the dipyrrinato ligand. Both the parent complex **1** and mesitylene derivatives **4**, **6**, and **7** emit at $\lambda_{em} = 672-677$ nm, whereas a small blue-shift ($\lambda_{em} = 658$ nm) and red-shift ($\lambda_{em} = 683-685$ nm) were observed for the methyl (**2**) and the phenyl substituted (**3** and **5**) complexes, respectively. The absence of any effect of the cyclometalating ligand, and the influence of the R substituent on λ_{max}, indicate that emission originates from the dipyrrinato ligand. Phosphorescence from the dipyrrinato ligand is further supported by the fact that cyclometalation at the 2′- or 6′-positions in **5** has minimal affect on the photophysical properties of the complexes. The emission spectrum for a regioisomeric mixture of **5** has a near identical line shape to that of **3**. The measured lifetime for the regioisomeric mixture of **5** can also be accurately fit to a single exponential decay, which implies identical decay constants for the excited state of each isomer. The assignment is consistent with DFT calculations that show the lowest triplet state localized on the dipyrrinato ligand (Figure 3b).

Phosphorescence from compounds containing a dipyrrinato ligand has rarely been directly observed. The phosphorescent spectra from BF_2(dipy) compounds has been reported at 77 K with the addition of iodoethane as a heavy atom solvent.[15] Triplet emission at 77 K has also been observed in a multicomponent BF_2(dipy)−M(II) terpyridine complexes because of charge-separation followed by recombination (M = Ru),[13] or by triplet energy transfer (M = Pt),[14] resulting in a $^3\pi-\pi^*$ excited state localized on the dipyrrinato moiety. Similarly, a boron dipyrrinato chromophore appended to a $(ppy)_2$Ir(bpy) complex has been shown to display phosphorescence at 77 K through triplet energy transfer from the excited state of the Ir fragment.[46] For the series of complexes reported here, direct coordination of the dipyrrinato ligand to iridium, as in the previously reported (C^N)Pt(dipy) complexes,[16] facilitates efficient intersystem crossing to the triplet state and thus, phosphorescence from the dipyrrinato ligand is observed at room temperature.

The luminescent quantum efficiencies (Φ) of complexes **1**−**7** range from 0.06 to 0.115 at room temperature in deaerated solution. A pronounced difference in efficiency is seen between 5-phenyl substituted complexes **3** and **5** ($\Phi = 0.06$) versus the 5-mesityl derivatives **4**, **6**, and **7** ($\Phi = 0.09-0.115$). A related, albeit much larger, increase in quantum yield has also been observed in fluorescent zinc bis-dipyrrinato complexes when the phenyl group ($\Phi = 0.006$) is replaced with a mesityl group ($\Phi = 0.36$).[10] Detailed studies by Li et al. on related boron compounds concluded that the reduced efficiency is due to rotation of the aryl ring, accompanied by a corresponding puckering distortion of the dipyrrinato ligand. The distortion results in an excited-state conformer that undergoes facile non-radiative deactivation to the ground state.[31,45] A similar deactivation pathway, albeit less pronounced, is most likely active in the aryl substituted complexes **3**−**7**. This conclusion is supported by the lower efficiency and shorter lifetimes in **3** and **5** as compared to **4**, **6**, and **7**. The effects of aryl rotation can also be observed when comparing the differing response of emission behavior to solvent rigidity. While the excited state lifetimes of **4**, **6**, and **7** double upon cooling to 77 K, a 3-fold increase in lifetime is found for **3** and **5**, presumably because of the rigid environment hindering rotation of the phenyl group. Similar behavior is also observed at room temperature when the photophysical properties of complexes **3** and **4** are examined in rigid media (polymethylmethacrylate, PMMA, Supporting Information, Figure S22). The radiative rates (k_r) of both **3** and **4** remain constant upon doping in PMMA (2%, w/w). However, while the non-radiative rate (k_{nr}) of the mesityl derivative (**4**) is unchanged in PMMA, the k_{nr} of the phenyl derivative (**3**) is lowered from 1.8 to 1.1×10^5 s^{-1} (Table 2) resulting in an increased efficiency ($\Phi = 0.092$). Again, this behavior coincides with the rigid media inhibiting the rotation of the phenyl ring and thus, decreasing the rate of non-radiative deactivation to the ground state.

Complexes **1**−**7** have relatively high non-radiative rates ($k_r \sim 1 \times 10^5$ s^{-1}) and display only a minimal increase ($\times 2-3$) in lifetime upon cooling from room temperature to 77 K. Similar behavior has also been observed for the red phosphor, bis[2-(2′-benzothienyl)pyridinato-N,C3′]-iridium acetylacetonate, and is attributed to an intrinsic temperature-independent non-radiative decay process.[47,48] Temperature-independent non-radiative processes typically involve geometric distortions caused by low energy molecular vibrations of the emissive ligand.

Dipyrrins can roughly be described as being half of a porphyrin ring, and the triplet emission energies for complexes **1**−**7** are comparable to those of Pt(porphyrins).[49] Despite this similarity, phosphorescent emission from Ir(5-Ph-dipy) **3** ($\Phi = 0.06$) is less than one-third as efficient than from platinum tetraphenylporphyrin (PtTPP, $\Phi = 0.19$).[49] A comparison of radiative and non-radiative rates between **3** and PtTPP shows higher values for both rates in **3** ($k_r = 1.1 \times 10^4$ s^{-1}; $k_{nr} = 1.8 \times 10^5$ s^{-1}) than in PtTPP ($k_r = 3.5 \times 10^3$ s^{-1}; $k_{nr} = 1.5 \times 10^4$ s^{-1}).[49] The difference in quantum yields is therefore caused by the 10-fold higher k_{nr} values in **3**. A likely origin of the high non-radiative rates in **3** is the out-of-plane distortion of the pyrrole rings observed in

(46) Rachford, A. A.; Ziessel, R.; Bura, T.; Retailleau, P.; Castellano, F. N. *Inorg. Chem.* **2010**, *49*, 3730−3736.

(47) Tanaka, I.; Tabata, Y.; Tokito, S. *Jpn. J. Appl. Phys.* **2004**, *43*, 1601–1603.

(48) Endo, A.; Suzuki, K.; Yoshihara, T.; Tobita, S.; Yahiro, M.; Adachi, C. *Chem. Phys. Lett.* **2008**, *460*, 155–157.

(49) Atwater, B. *J. Fluoresc.* **1992**, *2*, 237–246.

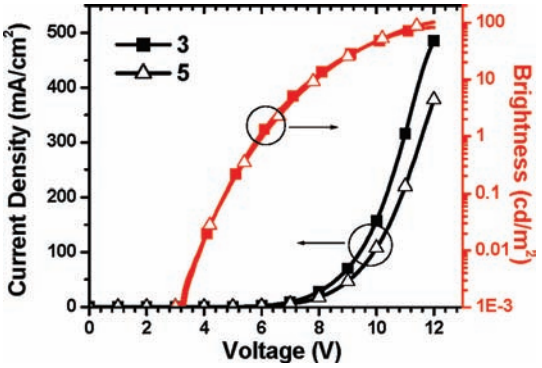

Figure 5. Luminance (red, cd/m^2) and current density (black, mA/cm^2) as a function of voltage (V) for OLEDs using compound **3** (filled squares) and **5** (open triangles).

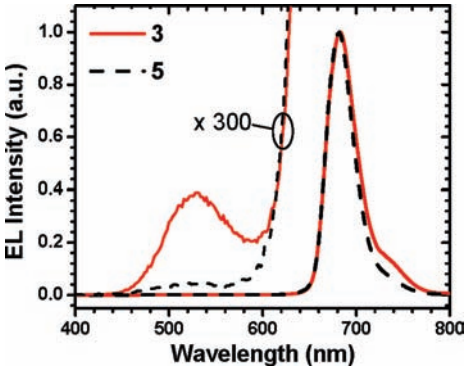

Figure 6. EL spectra of OLEDs using dopants **3** and **5**.

the crystal structures of **3**, **4**, and **5**(6′,6′) (Figure 2). The presence of both a planar and nonplanar form of the dipyrrinato ligand in the unit cell of **4** suggests a low energy barrier for this type of distortion. For Pt(TPP), on the other hand, the ability to traverse such a large amplitude distortion is limited by the structural rigidity of the porphyrin ring system.

OLED. Organic light emitting diodes (OLEDs) using complexes **3** and **5** as emissive dopants were fabricated by high-vacuum thermal evaporation. The device architecture, shown in Supporting Information, Figure S23, is identical to the one employed to make efficient OLEDs doped with Pt(octaethylporphyrin).[50] The voltage-current density and voltage-luminance characteristics of the fabricated OLEDs are shown in Figure 5. The turn-on voltages were 5.9 and 6 V for devices with an aluminum tris(8-hydroxyquinoline) (Alq_3) host doped with 10% **3** and **5**, respectively, and both reached a luminance of 100 cd/m^2 at 12 V. Both devices exhibited narrow, deep-red emission (λ_{max} = 682 nm) when positive bias was applied to the ITO electrode (Figure 6). The EL spectra are coincident with the photoluminescent (PL) spectra of the corresponding complexes at room temperature. However, for the device employing compound **3**, it was observed that, with increasing driving voltage, the EL color slowly evolved from deep saturated red, to orange to yellow. Examination of the EL spectra from this device shows that this perceived color change at higher voltage is due to mixed emission from both the phosphorescent dopant and Alq_3 host (Figure 6). In contrast, emission from Alq_3 is reduced significantly when **5** is used as the dopant. The decreased contribution from Alq_3 could be due to better hole trapping by the dopant since both the **5**(2′,6′) and **5**(6′,6′) isomers are easier to oxidize than dopant **3**. Improved charge trapping could also be responsible for the lower conductivity of devices doped with **5** compared to those doped with **3** (Figure 5). The maximum external quantum efficiency was 0.6% and 1.0% for the device using compound **3** and **5**, respectively (Supporting Information, Figure S24). The relatively poor device performance, especially when compared relative to other cyclometalated Ir-based devices, is likely due to the low solution photoluminescent efficiencies of the dopants.

(50) O'Brien, D. F.; Baldo, M. A.; Thompson, M. E.; Forrest, S. R. *Appl. Phys. Lett.* **1999**, *74*, 442–444.

Conclusion. In summary, a series of dipyrrinato-based bis-cyclometalated Ir(III) complexes has been synthesized and characterized. The electrochemical, spectroscopic, and electroluminescent properties were examined. The oxidation and reduction potentials of this series of molecules, with one exception, were found to be centered on the dipyrrinato ligand. Cyclometalation at the 6′-position of ooppz ligand results in a shift in the location of the HOMO from dipyrrinato to the cyclometalating ligand, and thus the oxidation potential is shifted to more negative potentials relative to the other molecules. All of the complexes have high molar absorptivity (10^4 M^{-1} cm^{-1}) at similar wavelengths (~480 nm) and exhibit phosphorescent emission at room temperature in the deep red part of the visible spectrum (658−685 nm) with quantum efficiencies ranging from 0.06 to 0.115. OLEDs made using two of the complexes as dopants had external quantum efficiencies of 0.6 and 1.0%.

Despite the modest quantum efficiency, particularly with respect to other cyclometalated iridium complexes, these derivatives provide efficient phosphorescence from a dipyrrinato ligand at room temperature. The $(C^{\wedge}N)_2$-Ir(dipy) complexes have several advantages not present in the fluorescent dipyrrinato analogues. (1) Selective monitoring of emission with no absorption spectra overlap is possible because of the large Stokes shift between absorption and emission maxima. (2) The red-shifted phosphorescent emission ($\lambda_{max} \approx 680$ nm) is in the biological tissue window (650−900 nm) making these complexes possible candidates for biological labeling applications. (3) Efficient triplet excited state formation upon photoexcitation is an important step in singlet oxygen formation for both oxygen sensing and photodynamic therapy. (4) The high energy absorption wavelength and oxidation potential of the complexes can easily be modified by changing the cyclometalating ligand with minimal affect on the photophysical properties of the dipyrrinato ligand.

Acknowledgment. The authors would like to thank Universal Display Corporation and the Department of Energy for their financial support of this work.

Supporting Information Available: The ^{1}H and ^{13}C NMR of **1**−**7**, crystallographic data for compounds **3**, **4**, and **5**(6′,6′), the CV traces of **3** and **5**, the absorption/emission spectra of **1**−**7**, and the room temperature emission spectra of **3** and **4** in PMMA. This material is available free of charge via the Internet at http://pubs.acs.org.